Original Article

TXNIP knockout improves cardiac function after myocardial infarction by promoting angiogenesis and reducing cardiomyocyte apoptosis

Jin Wang[1#], Xue-Jiao Wang[1#], Yan Zhang[1,2#], Wen-Juan Shi[1], Zhan-Dong Lei[1], Xiang-Ying Jiao[1]^

[1]Key Laboratory of Cellular Physiology (Shanxi Medical University), Ministry of Education, and the Department of Physiology, Shanxi Medical University, Taiyuan, China; [2]Department of Foreign Languages, Changzhi Medical College, Changzhi, China

Contributions: (I) Conception and design: XJ Wang, XY Jiao, J Wang, Y Zhang; (II) Administrative support: XY Jiao; (III) Provision of study materials or patients: XJ Wang, Y Zhang, WJ Shi, ZD Lei; (IV) Collection and assembly of data: XJ Wang, J Wang; (V) Data analysis and interpretation: XJ Wang, J Wang, Y Zhang; (VI) Manuscript writing: All authors; (VII) Final approval of manuscript: All authors.

[#]These authors contributed equally to this work.

Correspondence to: Dr. Xiang-Ying Jiao. Key Laboratory of Cellular Physiology (Shanxi Medical University), Ministry of Education, and the Department of Physiology, Shanxi Medical University, Taiyuan 030001, China. Email: jiaoxyty@163.com.

Background: Myocardial infarction (MI) is a common cause of death. Thioredoxin-interacting protein (TXNIP) expression increases after MI, and it exerts a negative regulatory effect on cardiac function after MI. Our study aimed to investigate the specific regulatory mechanism of TXNIP on angiogenesis and cardiomyocyte apoptosis after MI.

Methods: The *TXNIP* gene knock-in (*TXNIP*-KI) and knock-out (*TXNIP*-KO) mice were generated, respectively. Eight-week-old male *TXNIP*-KO, *TXNIP*-KI, and wild type (WT) mice were subjected to MI by permanent ligation of the left anterior descending artery. Cardiomyocyte apoptosis was detected by TUNEL assay on the 4th post-surgery day. The expressions of TXNIP, hypoxia-inducible factor-1α (HIF-1α), vascular endothelial growth factor (VEGF), phosphorylated protein kinase B (p-AKT), p-AMP-activated protein kinase (p-AMPK), cleaved caspase-3, and caspase-3 were detected by Western blot. Quantitative real-time PCR was performed to detect the expression of *TXNIP*, *HIF-1α*, *VEGF*, prolyl hydroxylase (*PHD*) 1, and factor inhibiting HIF (*FIH*). In addition, the superoxide dismutase (SOD) activity and malondialdehyde (MDA) level in each group were also measured. On day 7 after MI, the hearts of sacrificed animals were analyzed by immunohistochemistry to assess CD31 expression and determine the density of angiogenesis. One month after treatment, the cardiac functional and structural changes were determined by echocardiography and the level of myocardial fibrosis was observed by Masson staining.

Results: Compared with WT mice, *TXNIP*-KO mice had a significantly improved cardiac functional recovery after MI, and the proportion of myocardial fibrosis area was dramatically reduced, cardiomyocyte apoptosis was decreased, and angiogenesis was significantly increased; *TXNIP*-KI mice reversed in these changes. The expression of HIF-1α, p-AKT, and p-AMPK increased after MI in *TXNIP*-KO mice, and the mRNA expression of *PHD* 1 and *FIH* decreased. *TXNIP*-KI mice reversed in these changes.

Conclusions: After MI, TXNIP down-regulated the level of HIF-1α and VEGF, reduced the number of angiogenesis, increased cardiomyocyte apoptosis, and ultimately led to a poor prognosis of ischemic myocardium. TXNIP was a protein with negative effects after MI and was expected to be a target for the prevention and treatment of MI.

Keywords: Thioredoxin-interacting protein (TXNIP); myocardial infarction (MI); hypoxia-inducible factor-1α (HIF-1α); angiogenesis

^ ORCID: 0000-0003-1182-9052.

Submitted Nov 22, 2021. Accepted for publication Apr 02, 2022.
doi: 10.21037/cdt-21-732
View this article at: https://dx.doi.org/10.21037/cdt-21-732

Introduction

Myocardial infarction (MI) is a global health problem, which poses a major threat to human health. Although treatment strategies have been improving, the incidence and mortality of acute myocardial infarction (AMI) remain high (1,2). So, it is urgent to find effective ways to prevent and treat MI. It is well known that, preventing cardiomyocytes apoptosis reduces the myocardium injury induced by hypoxia/ischemia (3). Other studies also demonstrated that compensatory angiogenesis and establishment of bilateral blood supply after MI recover blood perfusion and improve cardiac function (4,5). However, the key proteins and key pathways that affect angiogenesis and cardiomyocyte apoptosis for improving the prevention, treatment, and prognosis of MI are still not very clear.

Thioredoxin-interacting protein (TXNIP) is an α-arrestin protein, also known as vitamin D3 up-regulated protein 1 (VDUP1) or thioredoxin binding protein-2 (TBP-2). It is currently the only known endogenous thioredoxin (Trx) binding inhibitor protein (6,7). TXNIP plays multiple roles in processes, such as apoptosis, reactive oxygen species (ROS) regulation, and inflammation by acting as scaffolds for several proteins (8). TXNIP is also involved in cell signaling transduction, and its transcription and stability are regulated by multiple mechanisms, so it is a potential therapeutic target for the relative diseases (9). Recent studies have found that in the myocardium of mice subjected to MI, the expression of TXNIP was elevated. After using a sequence-specific DNA enzyme to down-regulate *TXNIP* mRNA, the cardiomyocyte apoptosis was reduced and the cardiac function was improved (10). However, it remains unclear whether the increase in the expression of TXNIP induced by ischemia and hypoxia has an effect on myocardial angiogenesis.

Hypoxia-inducible factor (HIF) is a type of transcription factor mainly found in humans and mammals. It regulates oxygen balance and facilitates the adaptation of cells and tissues to low O_2 concentrations. Increased expression of HIF-1α during MI can induce the expression of vascular endothelial growth factor (VEGF) and increase angiogenesis (11-13). Huang *et al.* used genetic engineering methods to specifically knockout the *HIF-1α* in mouse cardiomyocytes and found that the contractility of the mouse myocardium was weakened and angiogenesis was decreased, suggesting that HIF-1α plays an important role in angiogenesis (14). In recent years, studies have found that in murine lung epithelial (MLE-12) cells, *TXNIP* knock-in inhibited the expression of HIF-1α under hypoxia and normoxia (15). The above results suggested that the increased expression of TXNIP in ischemic myocardium may affect the expression of HIF-1α, which in turn affects angiogenesis, and thus participates in the regulation of ischemic hypoxic myocardium, but it remains to be verified.

Under normoxic conditions, HIF-1α is mainly in the cytoplasm, and it has a half-life of less than 5 min. Prolyl hydroxylase (PHD) and asparagine hydroxylase [factor inhibiting HIF (FIH)] regulate the protein stability and transcription activity of HIF-1α respectively. PHD can make the proline residues in the HIF-1α molecule hydroxylated, and finally recognized and degraded by the proteasome, thus affecting the protein stability of HIF-1α (16). FIH inhibits the transcriptional activity of HIF-1α by blocking the binding of the transcription activation domain of HIF-1α to CREB binding protein (CBP)/p300 (17). However, the effect of TXNIP on the expression of PHD and FIH is still unclear. This investigation was aimed to clarify the specific underlying mechanisms.

Therefore, this study mainly explores the effect of TXNIP on angiogenesis after MI, and focuses on elucidating the specific mechanism of TXNIP and HIF-1α interaction, so as to provide new ideas for the prevention and treatment of MI. We present the following article in accordance with the ARRIVE reporting checklist (available at https://cdt.amegroups.com/article/view/10.21037/cdt-21-732/rc).

Methods

Animals

TXNIP knockout heterozygous mice (MGI: 1889549, GemPharmatech Co., Ltd., Jiangsu, China) and *TXNIP* knock-in heterozygous mice (MGI: 1889549, GemPharmatech Co., Ltd., Jiangsu, China) in the background of C57BL/6J were mated and reared, and

homozygotes were gradually obtained. The results of gene identification and primer sequences for PCR were shown in Figure S1 and Table S1. The exon 1–exon 8 was deleted in *TXNIP* knockout heterozygous mice (Figure S2A). The *TXNIP* knock-in heterozygous mice were made using CRISPR/Cas9 technology and the principle of homologous recombination, and the CAG-LSL-Txnip-P2A-EGFP-PolyA fragment was inserted at the H11 site (Figure S2B). They were all fed in the specific pathogen free (SPF) laboratory animal environmental facilities with 12 h light/dark cycles under standard room temperature (22±2 ℃) and free access to water and food. After PCR gene identification, we used a simple random sampling method (the randomization sequence was generated by a computer based random order generator) to divide mice into WT + sham operation (WT-Sham) group, WT + MI (WT-MI) group, *TXNIP*-KO + sham operation (KO-Sham) group, *TXNIP*-KO + MI (KO-MI) group, *TXNIP*-KI + sham operation (KI-Sham) group, and *TXNIP*-KI + MI (KI-MI) group. The animals enrolled in the experiment were male mice of 8 weeks old. Due to consideration of different time-point grouping, as well as the need for pathological sections and frozen tissues, and the death of mice after modeling, we assigned 30 model mice in each group. Experiments were in compliance with the guidelines for the management of animals for medical experiments issued by (No. 55) the Ministry of Health of the People's Republic of China and the guidelines for the management of experimental animals issued by Shanxi Medical University, and was approved by the Association of Animal Protection of Shanxi Medical University (No. SYDL 2022002). A protocol was prepared before the study without registration.

Animal treatment

The mice in the MI groups were anaesthetized with 3% isoflurane (RWD Life Science, Shenzhen, China) and intubated into the trachea; then, they were connected to a small animal ventilator for assisted breathing and recorded the electrocardiogram (ECG). After fully exposing the heart, the left anterior descending coronary artery was ligated with a 7-0 surgical silk suture about 1 mm from the lower edge of the pulmonary artery cone and the left appendage. Ligation was deemed successful when the anterior wall and the apex of the left ventricle turned pale, the heart beat was weakened, and the mouse ECG showed ST-segment elevation. Mice with no significant elevation in the ST segment of ECG and mice that died after modeling were not included in the later experiments. The mice in the sham operation groups were only treated by exposing the heart and passing the 7-0 surgical silk suture at about 1 mm between the pulmonary artery cone and the left appendage without ligating the left anterior descending branch. Then the chest was closed with 5-0 surgical suture, and the mice were routinely injected with penicillin to prevent infection. In order to exclude interference from other factors, we placed the model mice in exactly the same SPF laboratory animal environmental facilities.

TUNEL staining

Heart tissue was harvested 4 days after surgery, fixed in paraformaldehyde, embedded in paraffin, and finally, sliced into 5-μm serial sections. The sections were stained using a colorimetric TUNEL apoptosis assay kit (C1098, Beyotime Biotechnology, Shanghai, China) according to the manufacturer's instructions. Images were captured with Olympus BX51 upright microscope. Scale bar =50 μm. A total of 6 mice in each group were selected, 5–7 locations were randomly selected in each mouse, and the cardiomyocyte apoptosis rate near the MI area was calculated. Cardiomyocyte apoptosis rate [apoptotic index (AI); %] = number of apoptotic cardiomyocyte nuclei/total number of cardiomyocyte nuclei ×100%.

Western blot analysis

The heart tissue around the infarction area was taken from each sample, and the total protein was extracted with Whole Cell Lysis Assay kit (KGP250, KeyGEN BioTECH Corp., Ltd., Jiangsu, China). The nuclear and cytoplasmic protein was extracted with Nuclear and Cytoplasmic Protein Extraction Kit (KGP150, KeyGEN BioTECH Corp., Ltd., Jiangsu, China). BCA Protein Assay kit (KGP902, KeyGEN BioTECH Corp., Ltd., Jiangsu, China) was applied to measure the protein concentration. Proteins were subjected to SDS-PAGE gels (Bio-Rad, Shanghai, China), and transferred to polyvinylidene difluoride (PVDF) membrane (Millipore, Taufkirchen, Germany). After blocking with 5% non-fat milk or 5% bovine serum albumin (BSA), the membranes were incubated with specific primary antibodies including anti-TXNIP (ab188865, 1:2,000, Abcam, Cambridge, UK), anti-HIF-1α (ab2185, 1:1,000, Abcam, UK), anti-VEGF (ab51745, 0.5 μg/mL, Abcam, UK), anti-AKT (9272S, 1:1,000, Cell Signaling Technology, Massachusetts, USA),

Table 1 Primer sequence for PCR

Name	Sequence (5'-3')
TXNIP-F	5'-CAAGGGTCTCAGCAGTGCAAAC-3'
TXNIP-R	5'-AAGCTCGAAGCCGAACTTGTACTC-3'
HIF-1α-F	5'-GGACGATGAACATCAAGTCAGCA-3'
HIF-1α-R	5'-AGGAATGGGTTCACAAATCAGCA-3'
VEGF-F	5'-GTGCACTGGACCCTGGCTTTA-3'
VEGF-R	5'-GGTCTCAATCGGACGGCAGTA-3'
PHD 1-F	5'-GGCGCTGCATCACCTGTATCTA-3'
PHD 1-R	5'-GGCTTCACCTCATGTGGGTTC-3'
FIH-F	5'-TTAGCGAAGCCTCGGAGACAA-3'
FIH-R	5'-CTGGACCCTAAGGCACAAGGAC-3'
β-actin-F	5'-CACTATTGGCAACGAGCGGTTCCG-3'
β-actin-R	5'-ACGGATGTCAACGTCACACT-3'

FIH, factor inhibiting hypoxia-inducible factor; F, forward; R, reverse; *HIF-1α*, hypoxia-inducible factor-1α; *PHD*, prolyl hydroxylase; *TXNIP*, thioredoxin-interacting protein; *VEGF*, vascular endothelial growth factor.

anti-p-AKT (9271S, 1:1,000, Cell Signaling Technology, USA), anti-p-AMP-activated protein kinase (p-AMPK) (2535S, 1:1,000, Cell Signaling Technology, USA), anti-AMPK (5831S, 1:1,000, Cell Signaling Technology, USA), anti-cleaved caspase-3 (9664S, 1:1,000, Cell Signaling Technology, USA), anti-caspase-3 (9662S, 1:1,000, Cell Signaling Technology, USA) and anti-Lamin B1 (12987-1-AP, 1:10,000, Proteintech Group, Inc., Rosemont, USA) at 4 ℃ overnight. The secondary antibody (BA1054, 1:10,000, BOSTER Biological Technology Co. Ltd., Wuhan, China) was incubated for 2 h the next day. Then, ultra-sensitive enhanced chemiluminescence (ECL) chemiluminescence detection kit (SW134-01, SEVEN BIOTECH, Corp., Ltd., Beijing, China) was used to detect the bands on each membrane, which was then exposed by Bio-Rad ChemiDoc™ Touch Imaging System. Four to seven mice were selected in each group for this experiment. Image J software was used to analyze the gray value and all data were reported as ratios of density of the band of interest to density of β-actin.

Quantitative real-time PCR

Total RNA in left ventricular sections were extracted using Trizol kits (9108, TaKaRa Bio Inc., Kyoto, Japan), and then reversely transcribed into cDNA by QuantiTect Reverse Transcription Kit (RR047A, TaKaRa Bio, Inc., Japan). The mRNA levels of *TXNIP*, *HIF-1α*, *VEGF*, *PHD* 1, and *FIH* were determined with Power SYBR Green PCR Master Mix (RR820A, TaKaRa Bio Inc., Japan). Five mice were selected in each group for this experiment. β-actin were used as the internal reference. The fold changes were calculated with $2^{-\Delta\Delta Ct}$ method. PCR primer sequences are shown in *Table 1*.

Immunohistochemistry

The hearts were harvested 7 days after surgery, fixed in paraformaldehyde, embedded in paraffin, and finally sliced into 5-μm serial sections. Paraffin sections were routinely deparaffinized and hydrated. EDTA antigen retrieval solution was used for antigen retrieval. Endogenous peroxidase was blocked. Non-specific antigens were blocked by goat serum. Rabbit two-step detection kit (PV6001, ZSGB-BIO, Beijing, China) was used for the above steps. Anti-CD31 (ab182981, 1:2,000, Abcam, UK), anti-α-actin (23660-1-AP, 1:200, Proteintech Group, Inc., USA) and secondary antibodies were incubated. The reaction products (brown) were visualized with DAB Horseradish Peroxidase Color Development Kit (ZLI9017, ZSGB-BIO, Beijing, China). Finally, nuclei were stained with hematoxylin. Images were captured with Olympus BX51 upright microscope. Scale bar =100 μm. Five mice were selected in each group, and 3–5 sites were randomly selected from each mouse, and the angiogenesis near the MI area in each group was calculated.

Echocardiography

Serial M-mode echocardiographic images of mice subjected to 1–2% isoflurane anesthesia were obtained via a GE Vivid 7-Dimension Ultrasound at 1 month after MI surgery, and using a rectal temperature probe, body temperature was carefully maintained between 36.7 and 37.3 ℃ throughout the study. We used toothed forceps to pinch the toes or tails of the mice, and there was no response. At the same time, it was observed that the respiratory rate of the mice decreased, and the breathing was regular and mainly abdominal breathing. Hearts were viewed in the short axis at the level of the papillary muscles. Each measurement was obtained in M-mode. The left ventricular ejection fraction (LVEF) and the left ventricular fractional shortening (LVFS) were used as indicators of cardiac function. The left ventricular internal diameter at end systole (LVIDs), left ventricular

internal diameter at end diastole (LVIDd), left ventricular end systolic volume (LVESV), left ventricular end diastolic volume (LVEDV), left ventricular anterior wall thickness at end systole (LVAWs), left ventricular anterior wall thickness at end diastole (LVAWd), left ventricular posterior wall thickness at end systole (LVPWs), and left ventricular posterior wall thickness at end diastole (LVPWd) were used as indicators of the cardiac structure. Seven mice were selected in each group for this experiment. We measured 3 times in a row and took the average.

Masson trichrome staining

The hearts were harvested 30 days after surgery, fixed in paraformaldehyde, embedded in paraffin, and finally sliced into 5-μm serial sections. The heart tissue section at the same layer was taken from each group, and the experiment was carried out according to the procedure of Masson staining kit (D026-1-3, Nanjing Jiancheng Bioengineering Institute, Nanjing, China). Four mice were selected in each group for this experiment. Images were captured with Nikon Ni-SS upright microscope.

Superoxide dismutase (SOD) activity

Firstly, 0.02 g of heart tissue around the infarction area was taken from each sample. Then added 9 times the volume of normal saline according to the ratio of weight (g): volume (mL) =1:9. Tissue homogenates were prepared using a tissue grinder. The tissue homogenate was centrifuged at 2,800 rpm/min for 10 min. Finally, we got 10% homogenate supernatant. Next, we measured the protein concentration by the BCA Protein Assay kit (KGP902, KeyGEN BioTECH Corp., Ltd., Jiangsu, China). The 10% tissue homogenate supernatant was diluted 100 times and the subsequent experiments were carried out according to the steps of the SOD assay kit (A001-3-2, Nanjing Jiancheng Bioengineering Institute, Nanjing, China.). Finally, we got the absorbance value and calculate the SOD activity according to the formula. Five mice were selected in each group for this experiment.

Malondialdehyde (MDA) level

In the same way as above, we first obtained 10% tissue homogenate supernatant. Afterwards, the experiment was carried out according to the steps of the MDA assay kit (A003-1-2, Nanjing Jiancheng Bioengineering Institute, Nanjing, China). Finally, the content of MDA was calculated according to the formula. Five mice were selected in each group for this experiment.

Statistical analysis

Statistical analysis was performed using the GraphPad Prism 6 software (GraphPad Software, Inc., San Diego, CA, USA). All data are presented as mean ± standard error of the mean (SEM). Differences were confirmed by one-way ANOVA. And $P<0.05$ indicated that the difference was statistically significant. All experiments were repeated three times independently.

Results

Establishment of MI model and the expressions of TXNIP gene at mRNA and protein levels in the myocardial tissues of mice with MI

After successfully ligating the left anterior descending coronary artery of the mice, the anterior wall of the left ventricle and the apex turned ischemic and white, the heart beat was weakened, and the ECG showed ST-segment elevation, indicating that the MI model was successfully constructed (*Figure 1A*). In the WT-MI group, the ST-segment in ECG of 2 mice was not elevated, and 3 mice died within the first 24 hours. In the KO-MI group, the ST-segment in ECG of 3 mice was not elevated, and 2 mice died within the first 24 hours. In the KI-MI group, the ST-segment in ECG of 1 mouse was not elevated, and 4 mice died within the first 24 hours. In the WT-Sham, KO-Sham and KI-Sham group, all animals survived until sacrifice. Mice with no significant elevation in the ST segment of ECG and mice that died after modeling were not included in the later experiments.

Four days after operation, tissues around MI were taken to detect the mRNA and protein expression of *TXNIP*. The expression of *TXNIP* in the KI-Sham group was significantly higher than that in the WT-Sham group ($P<0.05$, n=5). The *TXNIP* mRNA and protein expressions of WT-MI group and KI-MI group were respectively and significantly higher than those in their corresponding sham operation group ($P<0.05$, n=5). And the expression of TXNIP in the KI-MI group was significantly higher than that in the WT-MI group ($P<0.05$, n=5) (*Figure 1B,1C*). *TXNIP*-KO mice were *TXNIP* knockout mice, so the mRNA or protein expression of *TXNIP* in either the sham group or the MI group was almost close to zero. The above results suggest that the expressions of TXNIP increased after MI.

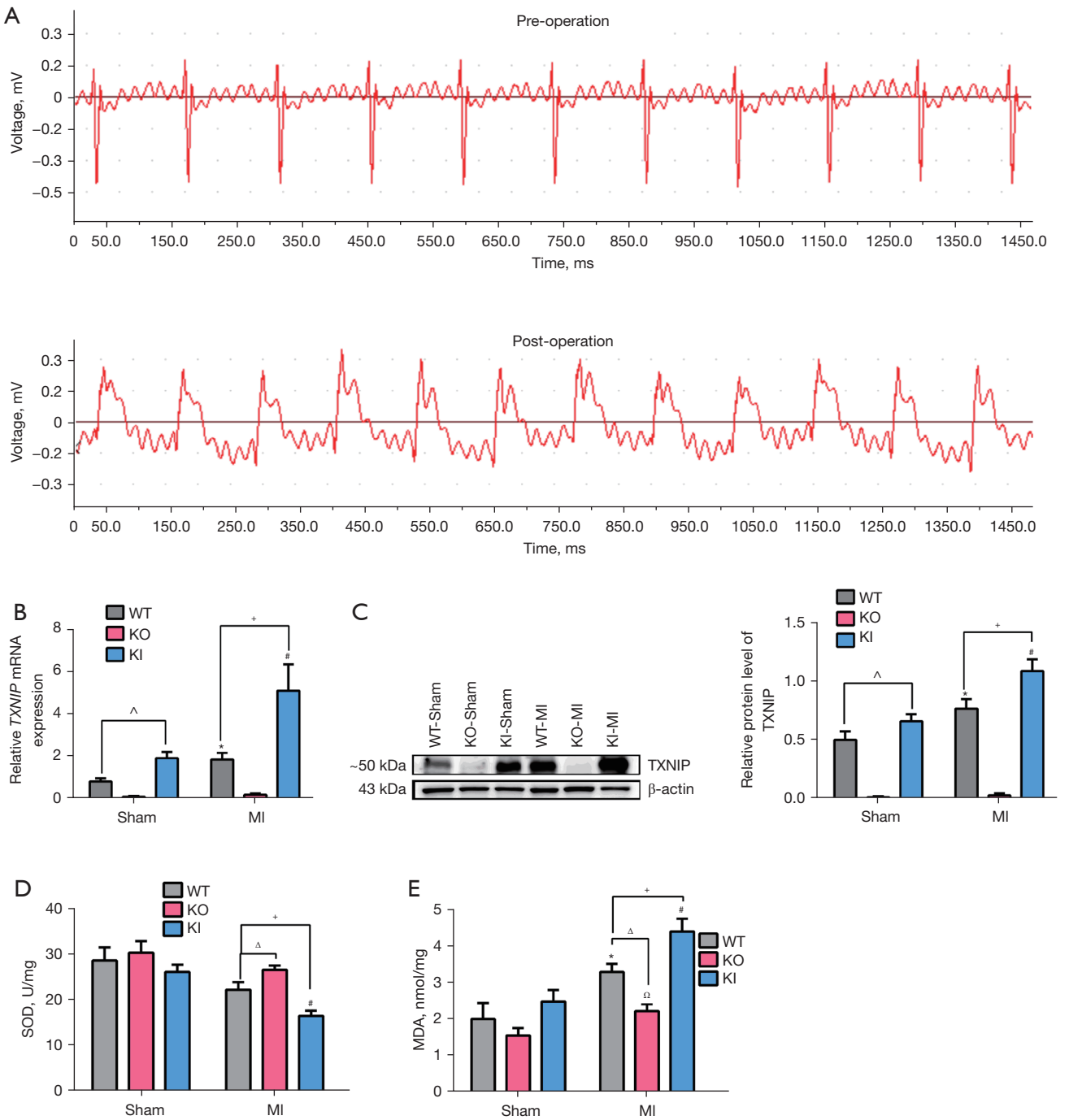

Figure 1 Successful establishment of mouse MI model. (A) ECG. (B) The mRNA expression of *TXNIP* detected by real-time PCR. Mean ± SEM, n=5. (C) The protein expression of TXNIP detected by Western blot. Mean ± SEM, n=5. (D) SOD activity of mice in each group. Mean ± SEM, n=5. (E) MDA levels of mice in each group. Mean ± SEM, n=5. *, P<0.05, WT-MI *vs.* WT-Sham; #, P<0.05, KI-MI *vs.* KI-Sham; +, P<0.05, KI-MI *vs.* WT-MI; ^, P<0.05, KI-Sham *vs.* WT-Sham; Ω, P<0.05, KO-MI *vs.* KO-Sham; Δ, P<0.05, KO-MI *vs.* WT-MI. ECG, electrocardiogram; KI, knock-in; KO, knock-out; MDA, malondialdehyde; MI, myocardial infarction; SEM, standard error of the mean; SOD, superoxide dismutase; TXNIP, thioredoxin-interacting protein; WT, wild type.

SOD activity and MDA levels of mice in each group

Four days after operation, tissues around MI were taken to detect SOD activity and MDA levels. The SOD activity of the KI-MI group was significantly lower than that of the KI-Sham group. Compared with the WT-MI group, the SOD activity in the KO-MI group was significantly increased, while that in the KI-MI group was significantly decreased (P<0.05, n=5) (*Figure 1D*). The levels of MDA in the WT, KO and KI groups were significantly increased after MI, and the differences were statistically significant. Compared with the WT-MI group, the MDA level in the KO-MI group was significantly decreased, while that in the KI-MI group was significantly increased (P<0.05, n=5) (*Figure 1E*).

TXNIP gene knockout improved left ventricular function after MI and reduced the myocardial fibrosis area

Left ventricular functional parameters were studied by echocardiography 30 days after surgical procedure (*Figure 2A-2K*). The results showed that all items were close to each other in sham group, with no significant difference. Among the MI groups, compared with the WT-MI group, LVEF, LVFS and LVAWs in the KI-MI group were lower, but LVIDs was higher, and the difference was statistically significant (P<0.05, n=7); by contrast, LVEF and LVFS increased significantly in KO-MI group (P<0.05, n=7), and LVIDs decreased significantly in KO-MI group (P<0.05, n=7). Although other indicators have a certain trend of change, but there was no statistical difference. The heart rate of mice in each group was measured and it is found that although there was a slight increase after surgery, there was no statistical difference (*Figure 2L*).

Masson staining was used to detect the percentage of cardiac fibrosis in each group (*Figure 3A*). Blue indicated fibrotic myocardial tissue and red indicated normal myocardial tissue. It was investigated that the fibrosis area in the three sham group only accounted for a very low percentage of the total area, even no fibrosis occurred. Compared with the WT-MI group, the percentage of the fibrosis area to the total area of the layer in the KI-MI group increased, while significantly decreased in the KO-MI group (P<0.05, n=5).

The heart was harvested 30 days after operation, and the weight of the mouse and the heart was detected. There was no significant difference in the body weight of the mice in each group (*Figure 3B*). The results showed that the heart weight to body weight ratio of the KI-MI group was significantly higher than that of the WT-MI group, while this ratio of the KO-MI group was significantly lower than that of the WT-MI group (P<0.05, n=6) (*Figure 3C*).

The above results suggest that *TXNIP* knockout improved of left ventricular function after MI, reduced the area of myocardial fibrosis and the ratio of heart weight to body weight.

TXNIP gene knockout improved cardiomyocyte apoptosis after MI

The heart was harvested 4 days after surgery was processed by dehydration and paraffin-embedding. Then, the sections were stained using a colorimetric TUNEL apoptosis assay kit (*Figure 4A*). α-actin was used as a marker to identify the cardiomyocytes (Figure S3). The positive TUNEL staining in the KI-MI group was significantly higher than that in the WT-MI group, and the myocardial cell AI (%) was significantly increased (P<0.05, n=6). Compared with the WT-MI group, the number of brown-yellow cell nuclei in the KO-MI group was significantly reduced, and the AI (%) of cardiomyocytes was significantly reduced (P<0.05, n=6).

The expression of cleaved caspase-3/caspase-3, apoptosis-related proteins, was detected by Western blot, and the results showed that the ration of cleaved caspase-3/caspase-3 in the KO-MI group decreased, compared with the WT-MI group, while it was increased in the KI-MI group (P<0.05, n=4) (*Figure 4B*).

The above results indicate that TXNIP knockout reduced the level of cardiomyocyte apoptosis induced by MI.

TXNIP gene knockout promoted angiogenesis after MI

Heart tissues were collected 7 days after operation, and the blood vessel density of each group was detected by immunohistochemistry (*Figure 5A*). There was few angiogenesis in the three sham groups. Among the MI groups, when compared with the WT-MI group, the angiogenesis and the vessel density near the infarct area in the KI-MI group were significantly reduced. However, the angiogenesis and the micro-vessel density in the KO-MI group were significantly increased (P<0.05, n=5).

Meanwhile, we detected the expressions of VEGF at the mRNA and protein levels (*Figure 5B,5C*). Compared with the WT-MI group, the mRNA and protein expressions of VEGF in the KI-MI group were significantly reduced, while the expressions in the KO-MI group were significantly increased (P<0.05, n=5).

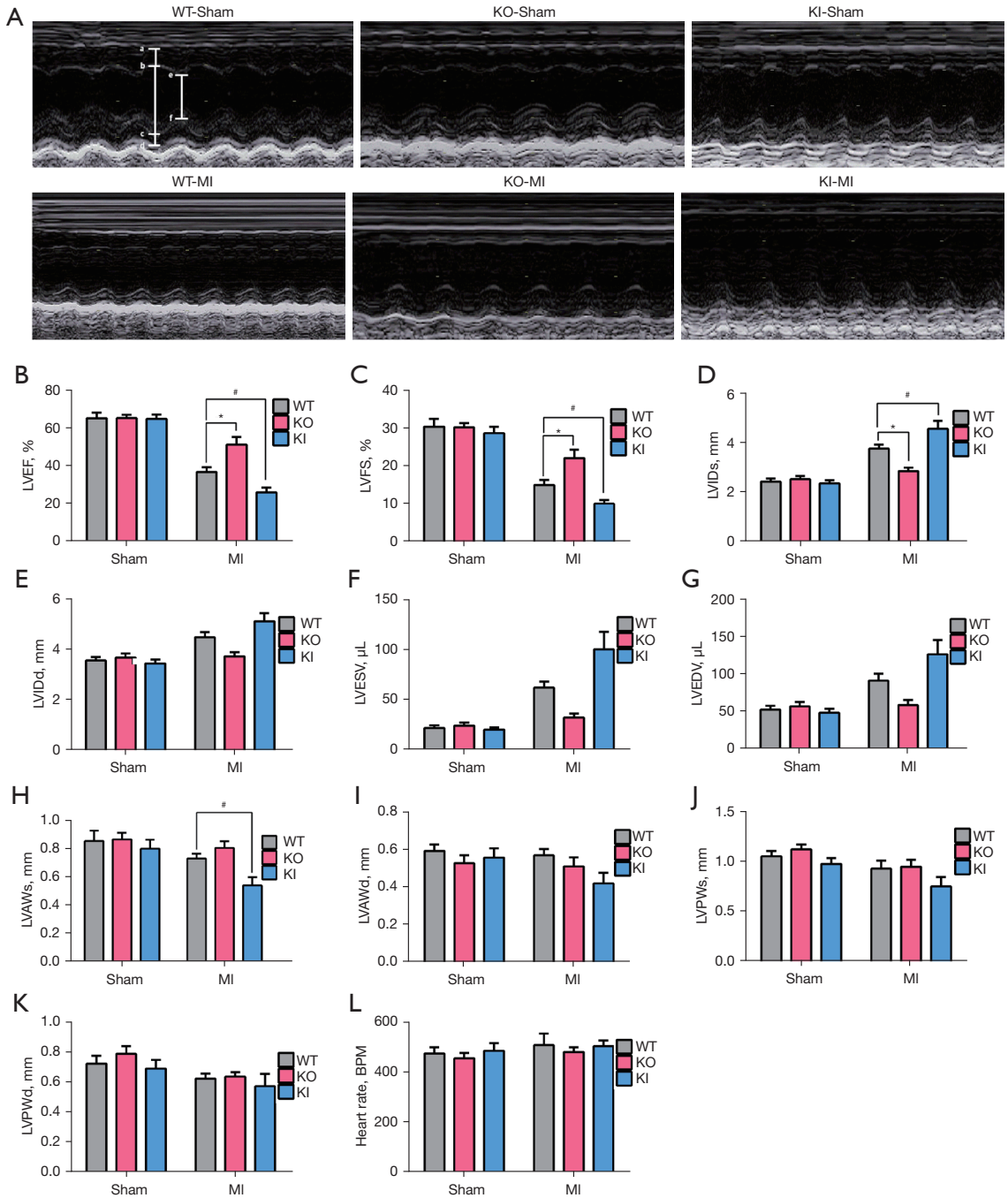

Figure 2 TXNIP aggravated left ventricular dysfunction after MI. (A) Representative echocardiographic M-mode images of each group at 30 days after surgery. a-b: left ventricular anterior wall thickness. b-c: LVIDd; c-d: left ventricular posterior wall thickness; e-f: LVIDs; (B-K) Statistical analysis of LVEF, LVFS, LVIDs, LVIDd, LVESV, LVEDV, LVAWs, LVAWd, LVPWs, and LVPWd. Mean ± SEM, n=7. (L) Heart rate of mice in each group. Mean ± SEM, n=7. *, P<0.05, KO-MI *vs.* WT-MI; #, P<0.05, KI-MI *vs.* WT-MI. KI, knock-in; KO, knock-out; LVAWd, left ventricular anterior wall thickness at end diastole; LVAWs, left ventricular anterior wall thickness at end systole; LVEDV, left ventricular end diastolic volume; LVEF, left ventricular ejection fraction; LVESV, left ventricular end systolic volume; LVIDd, left ventricular internal diameter at end diastole; LVIDs, left ventricular internal diameter at end systole; LVFS, left ventricular fractional shortening; LVPWs, left ventricular posterior wall thickness at end systole; LVPWd, left ventricular posterior wall thickness at end diastole; MI, myocardial infarction; SEM, standard error of the mean; TXNIP, thioredoxin-interacting protein; WT, wild type.

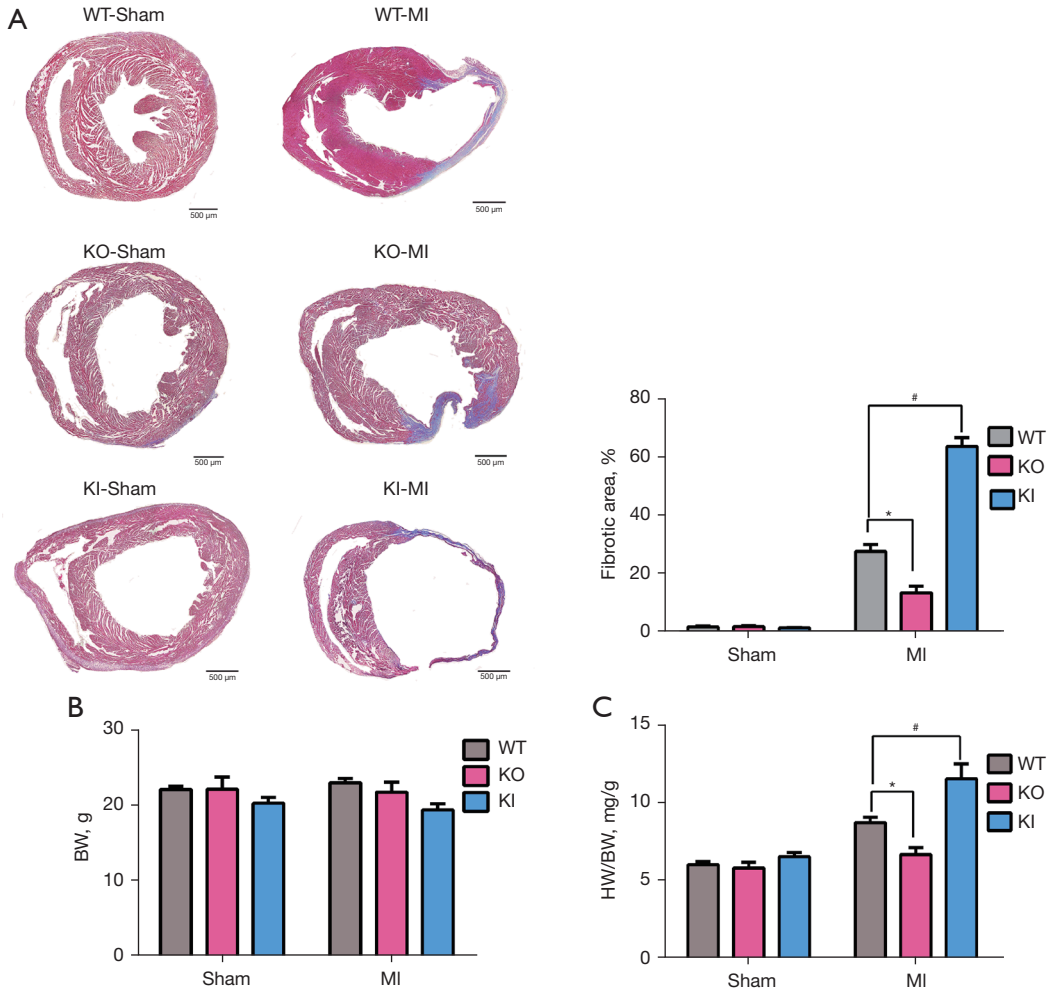

Figure 3 TXNIP increased the proportion of myocardial fibrosis area. (A) Masson trichrome staining of the heart 30 days after treatment. Scale bar =500 μm. Mean ± SEM, n=4. (B) BW of mice in each group. Mean ± SEM, n=6. (C) The ratio of HW to BW (HW/BW). Mean ± SEM, n=6. *, P<0.05, KO-MI *vs.* WT-MI; #, P<0.05, KI-MI *vs.* WT-MI. BW, body weight; HW, heart weight; KI, knock-in; KO, knock-out; MI, myocardial infarction; SEM, standard error of the mean; TXNIP, thioredoxin-interacting protein; WT, wild type.

The above results show that *TXNIP* knockout increased angiogenesis after MI.

TXNIP gene knockout increased the expression of HIF-1α

The expressions of p-AKT, p-AMPK, and HIF-1α in the hearts obtained 4 days after surgery were detected by Western blot. We measured the expression of p-AKT and p-AMPK in total protein and the expression of HIF-1α in nuclear protein (*Figure 6A*). The proof of successful nuclear protein extraction was in Figure S4. There was no significant difference in the expressions of p-AKT, p-AMPK and HIF-1α in the sham groups. Among the MI groups, when compared with the WT-MI group, the expression of p-AKT, p-AMPK, and HIF-1α in the KO-MI group increased, but the expression in the KI-MI group decreased significantly (P<0.05, n=4–7). To further confirm the effect of TXNIP on the expression of HIF-1α, the mRNA expression of *HIF-1α*, *PHD* 1, and *FIH* was then detected by real-time PCR (*Figure 6B-6D*). There was no significant difference in the mRNA expressions of *PHD* 1, *FIH* and *HIF-1α* in the sham groups. Among the MI groups, compared with the WT-MI group, the mRNA expression of *HIF-1α* was increased in the KO-MI group and the mRNA expressions of *PHD* 1 and *FIH* were decreased. In the KI-MI group, the mRNA expression of *HIF-1α* was

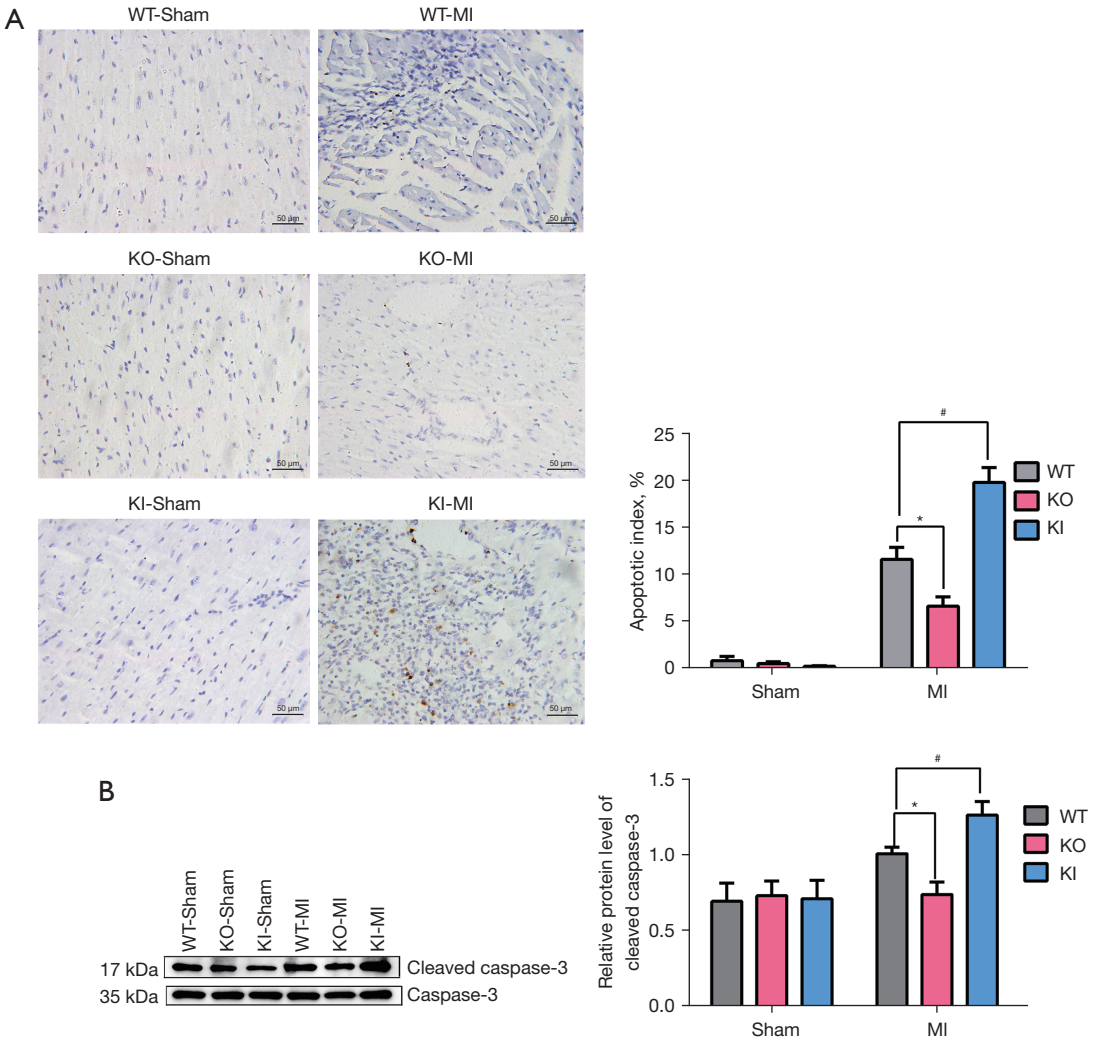

Figure 4 TXNIP increased cardiomyocyte apoptosis after MI. (A) TUNEL staining in each group 4 days after surgery. Scale bar =50 μm. Mean ± SEM, n=6. (B) The protein expression of cleaved caspase-3/caspase-3 detected by Western blot. Mean ± SEM, n=4. *, P<0.05, KO-MI *vs.* WT-MI; #, P<0.05, KI-MI *vs.* WT-MI. KI, knock-in; KO, knock-out; MI, myocardial infarction; SEM, standard error of the mean; TXNIP, thioredoxin-interacting protein; WT, wild type.

decreased but the mRNA expressions of *PHD* 1 and FIH were increased (P<0.05, n=5).

In summary, *TXNIP* knockout promoted the expression of *HIF-1α* at the transcription and protein levels, and *TXNIP* knock-in inhibited the expression of *HIF-1α* at the transcription and protein levels.

Discussion

MI is a common and frequently encountered clinical disease. It is a cardiac dysfunction or organic disease caused by coronary artery stenosis and insufficient blood supply (1,2). Reducing cardiomyocyte apoptosis and promoting angiogenesis are both important means to improve the function of ischemic myocardium and improve the prognosis of infarcted myocardium (3-5).

TXNIP is a member of the α-arrestin protein family. It is ubiquitously expressed in various organs and tissues including the heart, lung, thymus, spleen, kidney, and skeletal muscle, indicating that it plays an important role in maintaining cell homeostasis in the body (18). Studies have shown that injecting a proper dose of *TXNIP* DNA enzyme

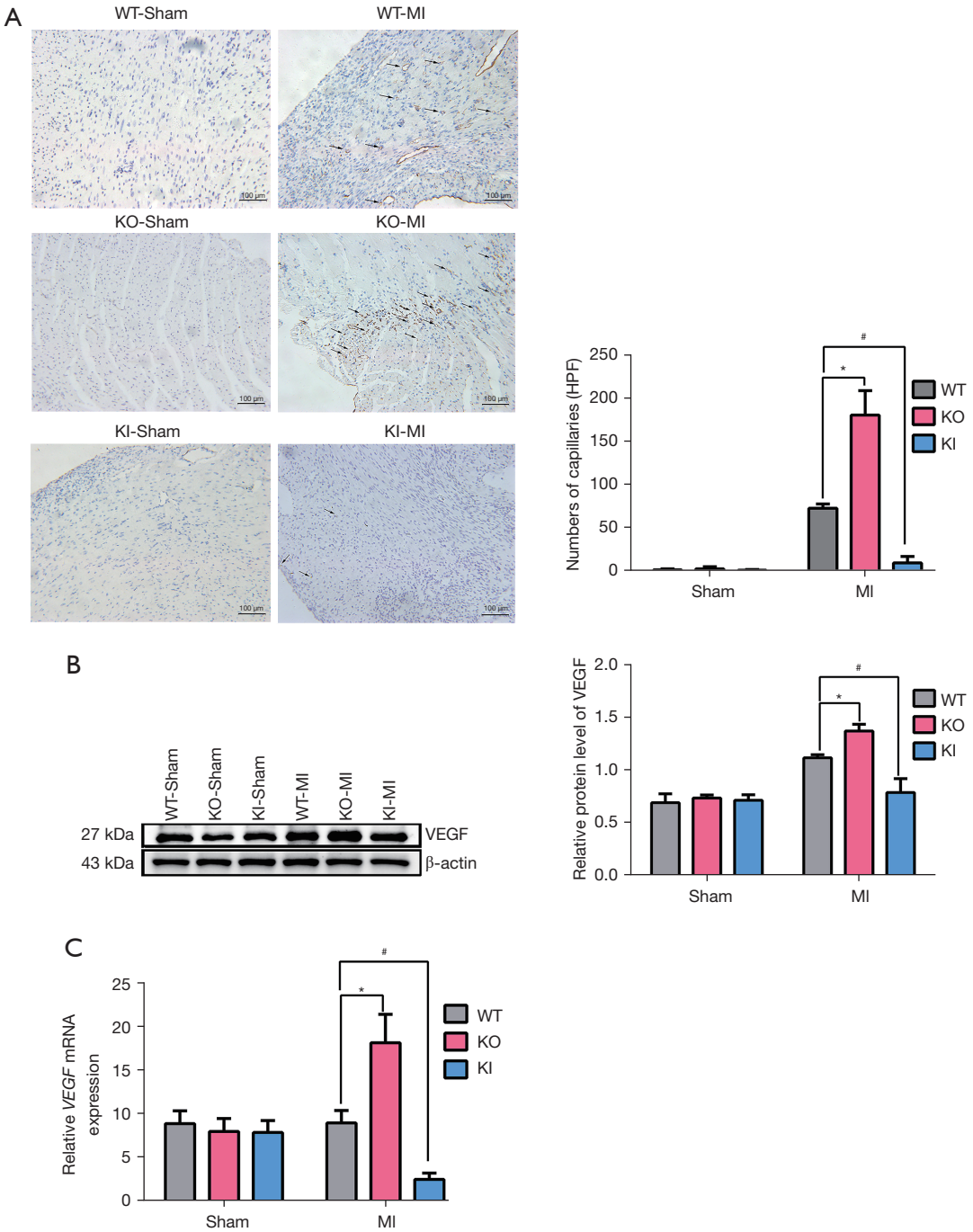

Figure 5 TXNIP reduced angiogenesis after MI. (A) Immunohistochemical staining of CD31 7 days after surgery. Scale bar =100 μm. Mean ± SEM, n=5. (B) The expression of VEGF detected by Western blot. Mean ± SEM, n=5. (C) The mRNA expression of *VEGF* detected by real-time PCR. Mean ± SEM, n=5. *, P<0.05, KO-MI *vs.* WT-MI; #, P<0.05, KI-MI *vs.* WT-MI. HPF, high power field; KI, knock-in; KO, knock-out; MI, myocardial infarction; SEM, standard error of the mean; TXNIP, thioredoxin-interacting protein; VEGF, vascular endothelial growth factor; WT, wild type.

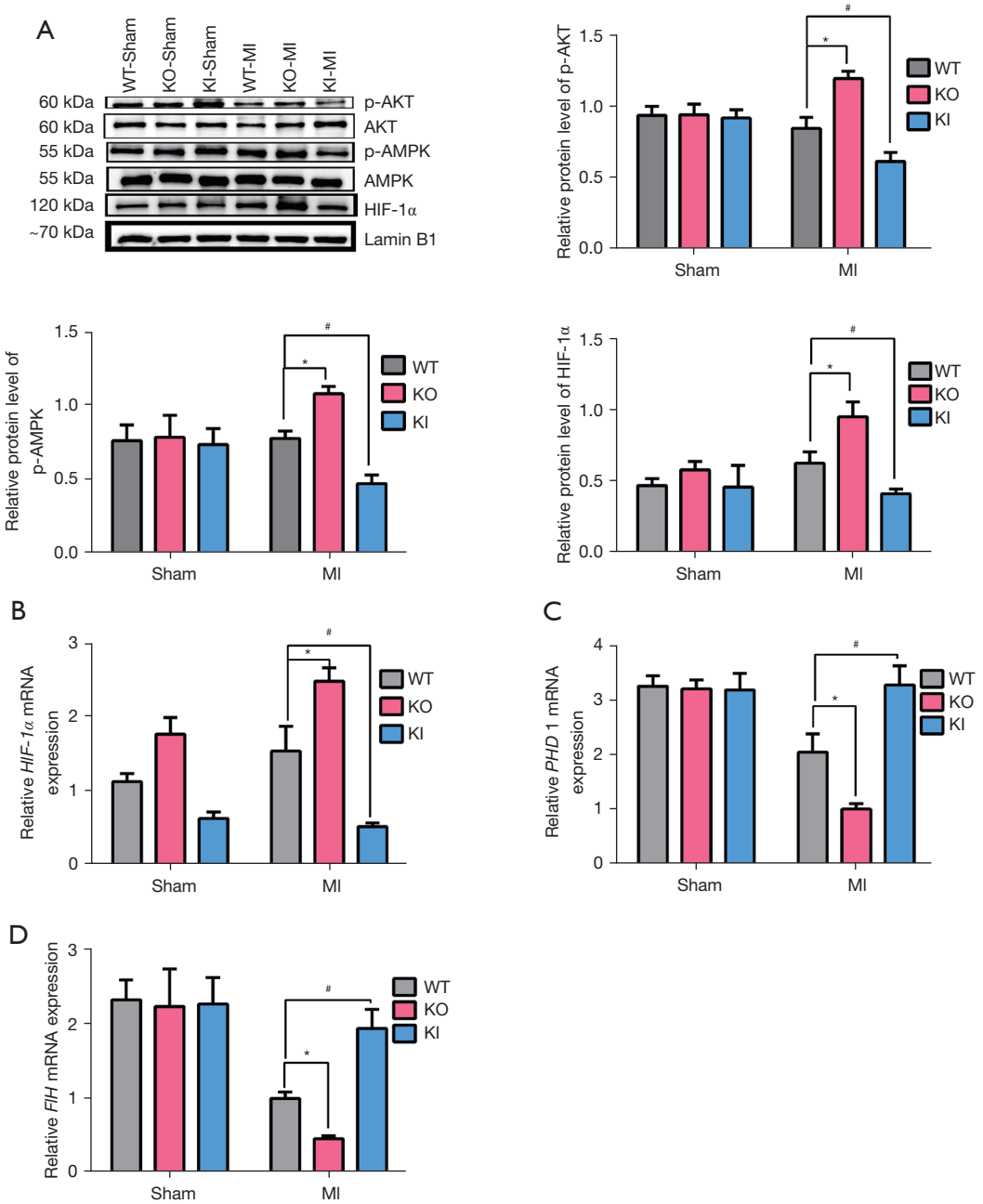

Figure 6 The mechanism of TXNIP regulating the expression of HIF-1α. (A) The expression of p-AKT, p-AMPK and HIF-1α in each group detected by Western blot. mean ± SEM, n=4–7. (B-D) The mRNA expression of *HIF-1α*, *PHD* 1, and *FIH* detected by real-time PCR. Mean ± SEM, n=5. *, P<0.05, KO-MI *vs.* WT-MI; #, P<0.05, KI-MI *vs.* WT-MI. AMPK, AMP-activated protein kinase; *FIH*, factor inhibiting hypoxia-inducible factor; HIF-1α, hypoxia-inducible factor-1α; KI, knock-in; KO, knock-out; MI, myocardial infarction; PHD, prolyl hydroxylase; SEM, standard error of the mean; TXNIP, thioredoxin-interacting protein; WT, wild type.

near the infarction area of the left ventricle in MI rats led to reduced cardiomyocyte apoptosis, collagen deposition, myocardial scar formation, and significantly improved left ventricular systolic and diastolic function (10). It was suggested that TXNIP has an important regulatory effect on the recovery of cardiac function and myocardial remodeling

after MI, and it is expected to become a target protein for the treatment of MI. We found in this study that the mRNA and protein levels of TXNIP were increased after MI, which was consistent with the finding from others that the expression of TXNIP in the heart of hypobaric hypoxia mice was increased in the decompression chamber (19). This suggested that TXNIP played a role in the dysfunction of ischemic myocardium. What's more, this study conducted MI models on the basis of constructing *TXNIP* knockout (*TXNIP*-KO) and *TXNIP* knock-in (*TXNIP*-KI) homozygous model mice. After operation, SOD activity and MDA level were measured in each group of mice 4 days after MI. We found that SOD activity decreased and MDA level increased after MI in each group of mice. Compared with the WT-MI group, the SOD activity in the KO-MI group was significantly increased, and the MDA level was significantly decreased. The KI-MI group was the opposite. It was proved that TXNIP promoted the increase of MDA level, reduced the activity of SOD, and promoted oxidative stress. TXNIP is a pro-oxidant molecule. It plays multiple important roles in ROS regulation. However, the ROS levels in the myocardial tissue of the mice in each group were not detected in this experiment, and the differences in the levels of ROS were not clear. Therefore, it is impossible to judge whether the regulation of TXNIP on angiogenesis was ROS-dependent or independent. This was a limit of this experimental, and we will continue to study it in depth in the future.

Small animal echocardiography was employed to detect the left ventricular function and Masson staining to detect fibrosis area. We found that all items were close to each other in sham group, with no significant difference. It is known that TXNIP is a glucose regulator. We measured the blood glucose level of normal 8-week-old WT, *TXNIP*-KO and *TXNIP*-KI mice and found that the blood glucose of *TXNIP*-KO mice was significantly lower than that of WT mice, but the blood glucose of *TXNIP*-KI mice was significantly higher than that of WT mice ($P<0.05$, $n=6$) (Figure S5). Referring to the echocardiography results of each group in the sham group, we found that although the blood glucose of each group of mice was different, it has not yet caused cardiac left ventricular dysfunction. Therefore, the differences in left ventricular function between the groups of mice after MI have nothing to do with the systemic phenotype of blood glucose. We also found in the *TXNIP*-KI mice that there were left ventricular dysfunction and increased fibrosis area after MI; while relatively improved left ventricular function and decreased fibrosis area in *TXNIP*-KO mice after MI. This indicated that TXNIP was a negative regulator for ischemic myocardium, which aggravated left ventricular dysfunction after MI. But the mechanism of its effect was still unclear.

On the one hand, increased apoptosis of cardiomyocytes is one of the main factors for the decline of cardiac function after MI (3). *In vitro* experiments confirmed that the enzymatic hydrolysis of TXNIP enhanced the combination of Trx and ASK1, thereby increasing the resistance of H9C2 cells to H_2O_2-mediated stress damage and reducing the apoptosis of H9C2 cells (10). TXNIP knock-in promoted peroxygen compounds production induced by high glucose and aggravated cardiomyocyte apoptosis (20). The above studies suggested that TXNIP plays an indispensable role in the process of regulating cardiomyocyte apoptosis (10). In this study, TUNEL staining was used to detect the apoptotic rate of cardiomyocytes, and Western blot was used to detect the expression level of cleaved caspase-3. We found that after MI, both the cardiomyocyte apoptotic rate and the cleaved caspase-3 expression were decreased in *TXNIP*-KO mice, while increased in *TXNIP*-KI mice. This proved that TXNIP increased the activity of caspase-3 and promoted the apoptosis of cardiomyocytes under ischemic conditions.

On the other hand, angiogenesis after MI is of great significance to the improvement of heart function. Exploring the effect of TXNIP on angiogenesis after MI is helpful to explain the negative effect of TXNIP on the cardiac function of ischemic myocardium (4). Some researchers have found in the study of human coronary artery endothelial cells that down-regulating the expression of TXNIP with siRNA promoted vascular endothelial migration and the formation of vascular networks (21,22). Fluid shear stress is the main trigger of angiogenesis. Normal laminar flow has been shown to promote angiogenesis by inhibiting the expression of TXNIP (23), suggesting that TXNIP is a regulator of biomechanical signals in the vascular system. So, what role does TXNIP play in angiogenesis after MI? VEGF is known to be an important mediator of angiogenesis. It acts as a powerful mitogen on endothelial cells and is one of the important proteins representing angiogenesis. In this experiment, we applied Western blot and real-time PCR to detect the level of VEGF. It was found that *TXNIP* knockout after MI increased VEGF expression, while *TXNIP* knock-in reduced VEGF expression. It is well known that CD31 is a marker protein of neonatal endothelial cells. In this experiment, CD31 immunohistochemical staining was

used to observe the effect of *TXNIP* knockout and knock-in on the number of new blood vessels in MI mice. It was found that the number of new blood vessels increased after *TXNIP* knockout, while decreased after *TXNIP* knock-in. The above results demonstrated that TXNIP inhibited angiogenesis after MI by inhibiting the expression of VEGF.

It is known that the expression of HIF-1α is increased in hypoxic tissues (11,12), and HIF-1α is a transcriptional regulator of VEGF, which affected angiogenesis by regulating VEGF (13). In order to confirm whether TXNIP inhibits angiogenesis through HIF-1α, this experiment detected the expression of HIF-1α in myocardial tissues by Western blot and Real-time PCR. It was found that the expression of HIF-1α in the KI-MI was significantly reduced and the expression of HIF-1α in the KO-MI group was increased, suggesting that TXNIP inhibited the expression of HIF-1α. Then, we continued to explore the specific mechanism of TXNIP's regulation of HIF-1α after MI. As we all know, the transcription and stability of HIF-1α are regulated by enzymes. At the transcription level, HIF inhibitor (FIH) inhibits the transcription activity of HIF-1α, thereby down-regulating the expression level of HIF-1α (17). At the protein level, HIF-1α is an unstable protein with a short half-life, even less than 5 minutes. PHD promotes the degradation of HIF-1α and reduce the protein level of HIF-1α, thereby affecting subsequent reactions. In this study, real-time PCR was used to detect the expression of *PHD* 1 and *FIH* in the MI model of *TXNIP* transgenic mice. It was found that the expression of *PHD* 1 and *FIH* in *TXNIP*-KO mice decreased after MI, while the expression of *PHD* 1 and *FIH* in *TXNIP*-KI mice increased. The results show that TXNIP affected the transcription and stability of HIF-1α by regulating the expression of *PHD* 1 and *FIH*. Some researchers have found that when AKT inhibitors were given after MI, the increase of HIF-1α was weakened. They also pointed out that activated AKT can promote the continuous activation of HIF-1α (24,25). In addition, AMPK's regulation of histone deacetylase 5 (HDAC5) protein phosphorylation and cytoplasmic shuttling is a key step in regulating the nuclear accumulation of HIF-1α protein and the subsequent hypoxia response (26). Therefore, we continued to investigate whether AKT and AMPK are involved in the regulation of HIF-1α by TXNIP. In this experiment, western blot was used to detect the expression of p-AKT and p-AMPK in both transgenic mice after MI. We found that *TXNIP* knockout promoted the expression of p-AKT and p-AMPK, while *TXNIP* knock-in inhibited the expression of p-AKT and p-AMPK. The above results indicated that TXNIP also affected HIF-1α by regulating the expression of p-AKT and p-AMPK. However, its specific mechanism needs to be further explored.

In summary, the current study has confirmed that TXNIP down-regulated the level of HIF-1α and the expression of VEGF, and reduced the number of angiogenesis after MI. At the same time, TXNIP promoted cardiomyocyte apoptosis. The above results ultimately led to poor cardiac prognosis. After MI, TXNIP inhibits HIF-1α by regulating the activation of AKT and AMPK and affecting the expression of *PHD* 1 and *FIH*. Since the mechanisms regulating angiogenesis and cardiomyocyte apoptosis after MI are complicated, our research may only clarify some of these mechanisms, and more efforts are needed in the future study.

Acknowledgments

The authors would like to acknowledge Xiao-Liang Wang (The Ohio State University College of Medicine) for the help in language editing.

Funding: This work was supported by the applied basic research project of Shanxi Province (No. 201901D111192), funds for Shanxi Key Subjects Construction (FSKSC), and Shanxi '1331 Project' Key Subjects Construction.

Footnote

Reporting Checklist: The authors have completed the ARRIVE reporting checklist. Available at https://cdt.amegroups.com/article/view/10.21037/cdt-21-732/rc

Data Sharing Statement: Available at https://cdt.amegroups.com/article/view/10.21037/cdt-21-732/dss

Peer Review File: Available at https://cdt.amegroups.com/article/view/10.21037/cdt-21-732/prf

Conflicts of Interest: All authors have completed the ICMJE uniform disclosure form (available at https://cdt.amegroups.com/article/view/10.21037/cdt-21-732/coif). The authors have no conflicts of interest to declare.

Ethical Statement: The authors are accountable for all aspects of the work in ensuring that questions related to the accuracy or integrity of any part of the work are appropriately investigated and resolved. Experiments were

in compliance with the guidelines for the management of animals for medical experiments issued by (No. 55) the Ministry of Health of the People's Republic of China and the guidelines for the management of experimental animals issued by Shanxi Medical University, and was approved by the Association of Animal Protection of Shanxi Medical University (No. SYDL 2022002). A protocol was prepared before the study without registration.

References

1. Núñez-Gil IJ, Riha H, Ramakrishna H. Review of the 2017 European Society of Cardiology's Guidelines for the Management of Acute Myocardial Infarction in Patients Presenting with ST-Segment Elevation and Focused Update on Dual Antiplatelet Therapy in Coronary Artery Disease Developed in Collaboration with the European Association for Cardio-Thoracic Surgery. J Cardiothorac Vasc Anesth 2019;33:2334-43.
2. Ibanez B, James S, Agewall S, et al. 2017 ESC Guidelines for the management of acute myocardial infarction in patients presenting with ST-segment elevation: The Task Force for the management of acute myocardial infarction in patients presenting with ST-segment elevation of the European Society of Cardiology (ESC). Eur Heart J 2018;39:119-77.
3. Wu T, Wu D, Wu Q, et al. Knockdown of Long Non-Coding RNA-ZFAS1 Protects Cardiomyocytes Against Acute Myocardial Infarction Via Anti-Apoptosis by Regulating miR-150/CRP. J Cell Biochem 2017;118:3281-9.
4. Narasimhan B, Narasimhan H, Lorente-Ros M, et al. Therapeutic angiogenesis in coronary artery disease: a review of mechanisms and current approaches. Expert Opin Investig Drugs 2021;30:947-63.
5. Wu R, Hu W, Chen H, et al. A Novel Human Long Noncoding RNA SCDAL Promotes Angiogenesis through SNF5-Mediated GDF6 Expression. Adv Sci (Weinh) 2021;8:e2004629.
6. Qayyum N, Haseeb M, Kim MS, et al. Role of Thioredoxin-Interacting Protein in Diseases and Its Therapeutic Outlook. Int J Mol Sci 2021;22:2754.
7. Alhawiti NM, Al Mahri S, Aziz MA, et al. TXNIP in Metabolic Regulation: Physiological Role and Therapeutic Outlook. Curr Drug Targets 2017;18:1095-103.
8. Hu J, Yu Y. The Function of Thioredoxin-Binding Protein-2 (TBP-2) in Different Diseases. Oxid Med Cell Longev 2018;2018:4582130.
9. Domingues A, Jolibois J, Marquet de Rougé P, et al. The Emerging Role of TXNIP in Ischemic and Cardiovascular Diseases; A Novel Marker and Therapeutic Target. Int J Mol Sci 2021;22:1693.
10. Xiang G, Seki T, Schuster MD, et al. Catalytic degradation of vitamin D up-regulated protein 1 mRNA enhances cardiomyocyte survival and prevents left ventricular remodeling after myocardial ischemia. J Biol Chem 2005;280:39394-402.
11. Gao S, Gao H, Dai L, et al. miR-126 regulates angiogenesis in myocardial ischemia by targeting HIF-1α. Exp Cell Res 2021;409:112925.
12. Wang R, Zhang Z, Xu Z, et al. Gastrin mediates cardioprotection through angiogenesis after myocardial infarction by activating the HIF-1α/VEGF signalling pathway. Sci Rep 2021;11:15836.
13. Hesse J, Groterath W, Owenier C, et al. Normoxic induction of HIF-1α by adenosine-A2B R signaling in epicardial stromal cells formed after myocardial infarction. FASEB J 2021;35:e21517.
14. Huang Y, Hickey RP, Yeh JL, et al. Cardiac myocyte-specific HIF-1alpha deletion alters vascularization, energy availability, calcium flux, and contractility in the normoxic heart. FASEB J 2004;18:1138-40.
15. Farrell MR, Rogers LK, Liu Y, et al. Thioredoxin-interacting protein inhibits hypoxia-inducible factor transcriptional activity. Free Radic Biol Med 2010;49:1361-7.
16. Gkagkalidis K, Kampantais S, Dimitriadis G, et al. Expression of HIF-2a in clear-cell renal cell carcinoma independently predicts overall survival. Med Mol Morphol 2020;53:229-37.
17. Pavlakis D, Kampantais S, Gkagkalidis K, et al. Hypoxia-Inducible Factor 2a Expression Is Positively Correlated With Gleason Score in Prostate Cancer. Technol Cancer Res Treat 2021;20:1533033821990010.
18. Nishiyama A, Matsui M, Iwata S, et al. Identification of thioredoxin-binding protein-2/vitamin D(3) up-regulated

protein 1 as a negative regulator of thioredoxin function and expression. J Biol Chem 1999;274:21645-50.
19. Karar J, Dolt KS, Mishra MK, et al. Expression and functional activity of pro-oxidants and antioxidants in murine heart exposed to acute hypobaric hypoxia. FEBS Lett 2007;581:4577-82.
20. Su H, Ji L, Xing W, et al. Acute hyperglycaemia enhances oxidative stress and aggravates myocardial ischaemia/reperfusion injury: role of thioredoxin-interacting protein. J Cell Mol Med 2013;17:181-91.
21. Dunn LL, Buckle AM, Cooke JP, et al. The emerging role of the thioredoxin system in angiogenesis. Arterioscler Thromb Vasc Biol 2010;30:2089-98.
22. Ng MK, Wu J, Chang E, et al. A central role for nicotinic cholinergic regulation of growth factor-induced endothelial cell migration. Arterioscler Thromb Vasc Biol 2007;27:106-12.
23. Patwari P, Chutkow WA, Cummings K, et al. Thioredoxin-independent regulation of metabolism by the alpha-arrestin proteins. J Biol Chem 2009;284:24996-5003.
24. Cuadrado I, Fernández-Velasco M, Boscá L, et al. Labdane diterpenes protect against anoxia/reperfusion injury in cardiomyocytes: involvement of AKT activation. Cell Death Dis 2011;2:e229.
25. Tsutsumi YM, Tsutsumi R, Mawatari K, et al. Compound K, a metabolite of ginsenosides, induces cardiac protection mediated nitric oxide via Akt/PI3K pathway. Life Sci 2011;88:725-9.
26. Salminen A, Kaarniranta K, Kauppinen A. AMPK and HIF signaling pathways regulate both longevity and cancer growth: the good news and the bad news about survival mechanisms. Biogerontology 2016;17:655-80.

Cite this article as: Wang J, Wang XJ, Zhang Y, Shi WJ, Lei ZD, Jiao XY. TXNIP knockout improves cardiac function after myocardial infarction by promoting angiogenesis and reducing cardiomyocyte apoptosis. Cardiovasc Diagn Ther 2022;12(3):289-304. doi: 10.21037/cdt-21-732

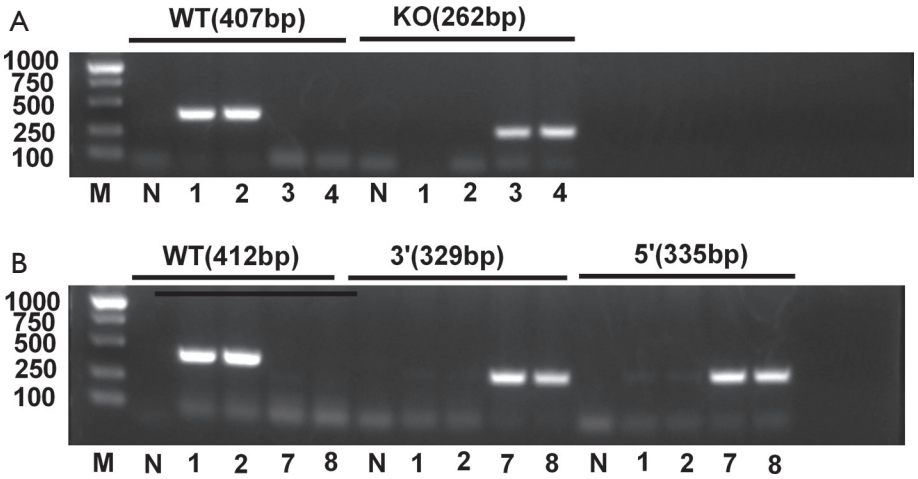

Figure S1 The results of gene identification. (A) Gene identification results of *TXNIP* gene knockout mice. (B) Gene identification results of *TXNIP* gene knock-in mice. KO, knock-out; M, marker; N, negative control; *TXNIP*, thioredoxin-interacting protein; WT, wild type.

Table S1 Primer sequences for PCR

Name	Sequence (5'-3')
TXNIP-KO-tF1A	AAGAGGAGTCCCCTGGATGAGGTT
TXNIP-KO-tR1A	AAGACAACGCCAGAAGGTCAGC
TXNIP-KO-WT-tF1A	CGCAACTTTCTGTCCAAGAAAGTG
TXNIP-KO-WT-tR1A	ATCGAGAAAAGCCTTCACCCAGT
TXNIP-KI-3'-rabbit-pA-tF1	CCTGCTGTCCATTCCTTATTCCATA
TXNIP-KI-3'-H11-tR3	ATATCCCCTTGTTCCCTTTCTGC
TXNIP-KI-5'-H11-tF3	GGGCAGTCTGGTACTTCCAAGCT
TXNIP-KI-5'-CAG-tR1	TGGCGTTACTATGGGAACATACGTC
TXNIP-KI-H11-wt-tF1	CAGCAAAACCTGGCTGTGGATC
TXNIP-KI-H11-wt-tR1	ATGAGCCACCATGTGGGTGTC

KI, knock-in; KO, knock-out; *TXNIP*, thioredoxin-interacting protein; WT, wild type.

https://dx.doi.org/10.21037/cdt-21-732

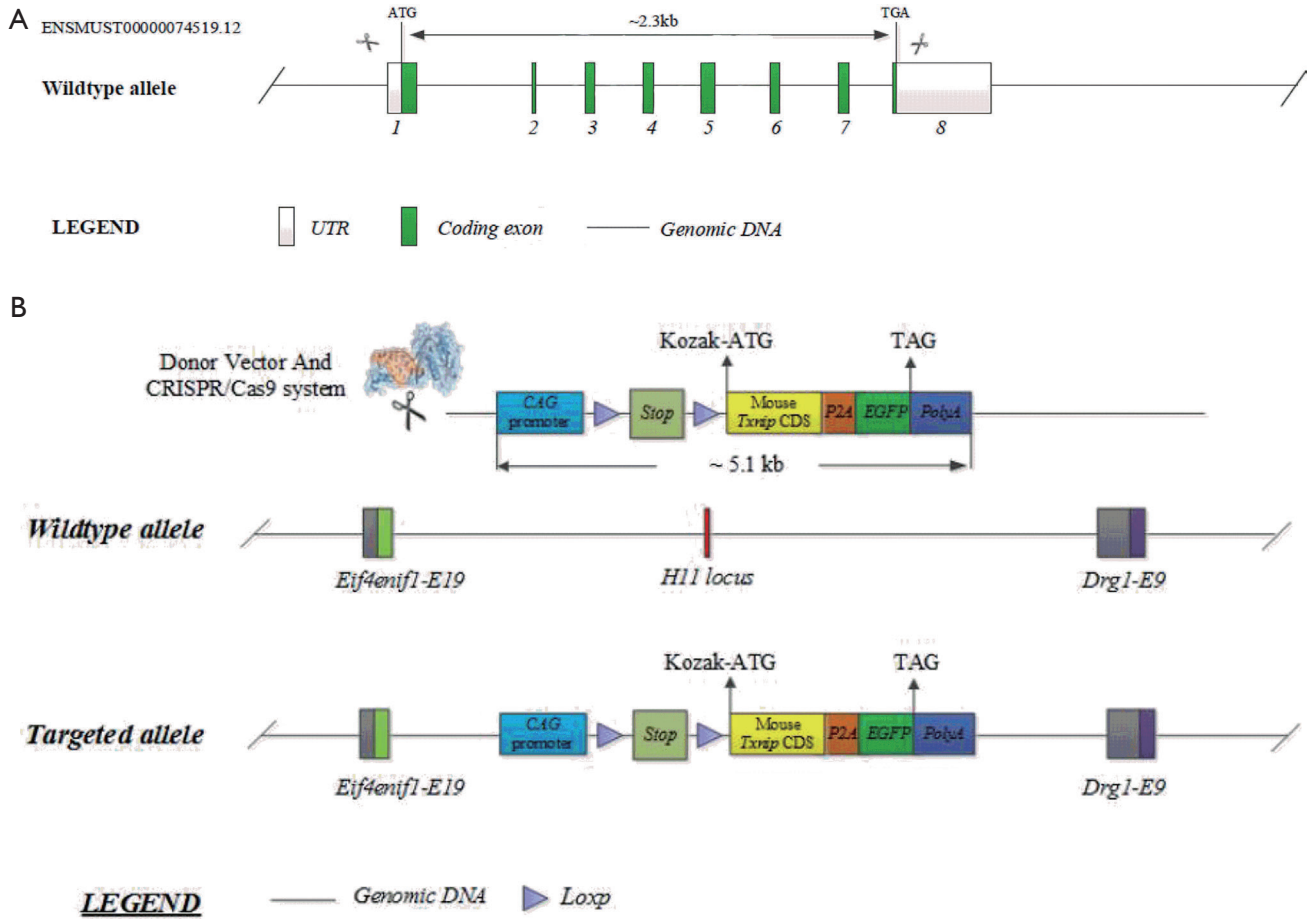

Figure S2 The project strategy map of transgenic mice. (A) The project strategy map of *TXNIP* knockout heterozygous mice. (B) The project strategy map of *TXNIP* knock-in heterozygous mice. *TXNIP*, thioredoxin-interacting protein; UTR, untranslated region.

https://dx.doi.org/10.21037/cdt-21-732

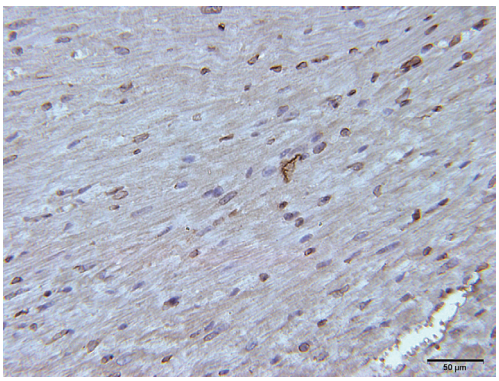

Figure S3 Immunohistochemical staining of α-actin in cardiomyocytes. Scale bar =50 μm.

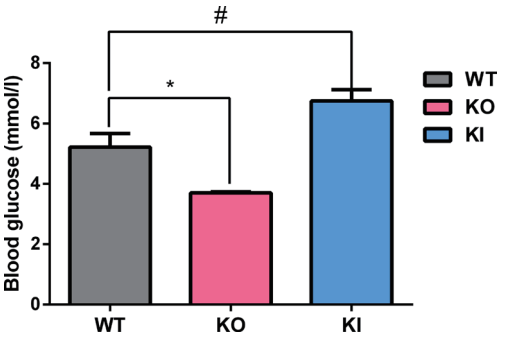

Figure S5 The blood glucose level of mice. Mean ± SEM, n=6, P<0.05. *, P<0.05, KO *vs.* WT; #, P<0.05, KI *vs.* WT. KI, knock-in; KO, knock-out; SEM, standard error of the mean; WT, wild type.

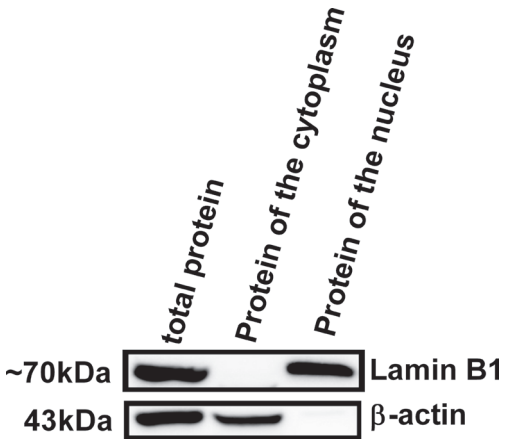

Figure S4 Expression of cytoplasmic reference and nuclear reference in each group.

https://dx.doi.org/10.21037/cdt-21-732